Article

Applied Spectroscopy

Applied Spectroscopy
2019, Vol. 73(10) 1146–1159

DOI: 10.1177/0003702819857139
journals.sagepub.com/home/asp
SAGE

Orientational Analysis of Monolayers at Low Surface Concentrations Due to an Increased Signal-to-Noise Ratio (S/N) Using Broadband Sum Frequency Generation Vibrational Spectroscopy

Narendra M. Adhikari*, Uvinduni I. Premadasa*, Zachary J. Rudy, and Katherine Leslee A. Cimatu

Abstract

Sum frequency generation (SFG) spectroscopy was used to deduce the orientation of the terminal methyl (CH_3) group of self-assembled monolayers (SAMs) at the air–solid and air–liquid interfaces at surface concentrations as low as 1% protonated molecules in the presence of 99% deuterated molecules. The SFG spectra of octadecanethiol (ODT) and deuterated octadecanethiol (d_{37} ODT) SAMs on gold were used for analysis at the air–solid interface. However, the eicosanoic acid (EA) and deuterated EA (d_{39} EA) SAMs on the water were analyzed at the air–liquid interface. The tilt angle of the terminal CH_3 group was estimated to be $\sim 39^\circ$ for a SAM of 1% ODT : 99% d_{37} ODT, whereas the tilt angle of the terminal CH_3 group of the 1% EA : 99% d_{39} EA monolayer was estimated to be $\sim 32^\circ$. The reliability of the orientational analysis at low concentrations was validated by testing the sensitivity of the SFG spectroscopy. A signal-to-noise (S/N) ratio of ~60 and ~45 was obtained for the CH_3 symmetric stretch (SS) of 1% ODT : 99% d_{37} ODT and 1% EA : 99% d_{39} EA, respectively. The estimated increase in S/N ratio values, as a measure of the sensitivity of the SFG spectroscopy, verified the capacity to acquire the SFG spectra at low concentrations of interfacial molecules under ambient conditions. Overall, the orientational analysis of CH_3 SS vibrational mode was feasible at low concentrations of protonated molecules due to increased S/N ratio. In support, the improved S/N ratio on varying incident power density of the visible beam was also experimentally demonstrated.

Keywords

Sum frequency generation spectroscopy, SFG, orientation, signal-to-noise ratio, S/N, power density, monolayer, interface

Date received: 7 September 2018; accepted: 12 May 2019

Introduction

Interfacial studies using sum frequency generation spectroscopy (SFG) are significant in many scientific studies such as colloidal chemistry, electrochemistry, catalysis, energetics, and bioanalytical chemistry.[1–8] Interfaces are asymmetric by nature[9] and have a net orientation of molecules which gives the interface different characteristics in comparison to the bulk. Past studies on molecular adsorption, molecular structure, and conformations have made significant contributions to understanding bio- and electrochemical properties of surfaces at air–solid and air–liquid interfaces. These studies gained attention in recent years due to their importance in many industrial applications and systems associated with biological phenomena.[10–13] The SFG was utilized to monitor the effects of hydration and other environmental factors to the head group conformation of the lipid component of lung surfactant by performing the orientational analysis. The findings are useful to understand the regulation of lung surfactant activity during inhalation and exhalation.[12]

Department of Chemistry and Biochemistry, Ohio University, Athens, OH, USA

*Equal contributors.

Corresponding author:
Katherine Leslee A. Cimatu, Ohio University, 100 University Terrace Boulevard, 136 Clippinger Labs, RM 295, Athens, OH 45701, USA.
Email: cimatu@ohio.edu

Sum frequency generation spectroscopy is a surface-specific technique that is nondestructive and label-free. The strength of SFG spectroscopy over other conventional spectroscopic methods is its ability to distinguish molecules at different interfaces due to the breaking of symmetry between two bulk phases. Thus, it is an ideal technique to study molecules at surfaces and interfaces. Sum frequency generation spectroscopy also provides information about the conformation, orientation, and interactions of interfacial molecules. Orientation analysis is an important aspect of SFG spectroscopy. The SFG signal from each vibrational mode depends on the orientation of the molecular group and its symmetry. Thus, the orientation can be obtained using the information deduced from the SFG spectra acquired in different polarization combinations. The orientational analysis is performed using spectral data from SSP, PPP, and SPS or PSS polarization combinations. The combination nomenclature follows the polarization state in the order of SFG, visible, and infrared (IR) beams, wherein SSP follows the arrangement of SFG, visible, and IR beams as S-polarized, S-polarized, and P-polarized, respectively. The S-polarization is perpendicular to the plane of incidence whereas P is parallel. The orientation analysis at the air–solid interface in this paper was obtained from the amplitude and intensity ratios between the CH_3 symmetric stretch (SS) and the antisymmetric stretch (AS) in the PPP polarization combination. On the other hand, the orientational analysis at the air–liquid interface was acquired by calculating the amplitude and intensity ratios between the CH_3 SS in SSP and SPS polarization combinations.[14,15]

Spectral fitting was carried out using Eq. 1, which includes the background, non-resonance, and broadband IR pulse shape terms. The details of the fitting are available in our earlier publications[14–17]

$$I_{SFG} = n_1 + e^{-\frac{(\omega-\omega_{IR})}{2(\delta\omega)^2}}\left|ne^{-i\varphi} + \sum\frac{A_q}{\omega_{IR}-\omega_q-i\Gamma_q}\right|^2 \quad (1)$$

where n_1 is the baseline correction factor, $\delta\omega$ is the spectral width of the broadband IR pulse, n is a nonresonant contribution, and φ is the nonresonant phase factor. A_q is the amplitude, ω_q is the vibrational frequency, and Γ_q is the peak width or damping constant of the vibrational mode q. The details about the theory and orientational analysis were reported in previous publications.[14–17]

The orientational analysis provides the tilt angle and distribution angle from the surface normal direction for different vibrational modes. Determination of the orientation of interfacial molecules is important to understand the surface phenomena such as catalysis, bio-membrane functions, adsorption, and reaction mechanisms.[18–21] The orientation information provides a detailed picture of the interfacial molecular conformations and their variations which, in turn, will help to understand the underlying mechanism and employ the surface processes to obtain the desired output. For example, studying the molecular conformations during the catalytic reaction will deliver information about the mechanism and eventually reveal a pathway to higher catalytic efficiency.

In this study, for the analysis at the air–solid interface, the orientation of the terminal methyl (CH_3) group of octadecanethiol (ODT) self-assembled monolayers (SAM) on gold was determined from 100% to a minimum of ~1% surface coverage of ODT (0.05 molecules/nm^2, assuming 0.21 nm^2 per alkanethiol molecule[22,23]). However, it is also important to first determine the current sensitivity of the SFG spectroscopy. Then the orientation of the molecules at lower concentrations can be validated, especially since the SFG intensity is known to decrease quadratically with the number of molecules on the surface. Herein, we determined the sensitivity of SFG spectroscopy by calculating the signal-to-noise (S/N) ratio as a function of surface concentration. To vary the surface concentration, isotopically labeled aliphatic compounds were utilized[23,24] and overall 100% surface coverage was constantly maintained. The results of the orientational analysis were reliable up to a 1% surface coverage of the protonated ODT SAMs on gold with an estimated S/N ratio of ~60.

For the analysis at the air–liquid interface, eicosanoic acid (EA) monolayers on the water surface were utilized and the orientation of the terminal CH_3 group was also determined at different surface concentrations. The SFG spectra were collected from 100% EA to a minimum of ~1% surface coverage of EA (0.15 molecules/nm^2). The orientation results were obtained for as low as 1% surface coverage of EA with 99% deuterated EA. However, the symmetric stretch of the terminal CH_3 group was still observed in the SFG spectrum of 1% EA : 99% d_{39} EA; thus, the S/N ratio value was estimated to be ~18. Additionally, the sensitivity was determined as a function of the power density of the incident beams.

Materials and Methods

Sum Frequency Generation Sample Preparation

For the air–solid interface, 1 mM ODT solution was used to deposit SAMs on gold films. The samples were prepared over 18 h from the solutions of ODT and d_{37} ODT containing 0% ODT : 100% d_{37} ODT, 1% ODT : 99% d_{37} ODT, 2% ODT : 98% d_{37} ODT, 4% ODT : 96% d_{37} ODT, 8% ODT : 92% d_{37} ODT, 16% ODT : 84% d_{37} ODT, 50% ODT : 50% d_{37} ODT, and 100% ODT : 0% d_{37} ODT. For the air–liquid interface, protonated and deuterated eicosanoic acid (EA) stock solutions were prepared in chloroform. Then, a series of solutions with different deuterated percentages (0% EA : 100 d EA, 1% EA : 99% d EA, 2% EA : 98% d EA, 16% EA : 84% d EA, 50% EA : 50% d EA, and 100% EA : 0% d EA) were prepared by mixing the calculated volumes of stock solutions. Table S1 in the Supplemental Material shows the concentration and

surface coverage of the protonated EA of the solution series. A volume of 25 μL of one solution was used to form a monolayer on deionized water (18 MΩ) in a clean glass petri dish. The sample was stabilized for 15 min for the SFG spectroscopic analysis. More experimental details are available in the online Supplemental Material.

Broadband Sum Frequency Generation

The details on the SFG spectroscopic system are reported in our previous publications.[14–17] Briefly, the one-box ultrafast Ti:sapphire oscillator system from Spectra-Physics (Solstice) was utilized to generate 100 fs pulses at 795 nm with the power of ~4 W before compression at a 1 kHz repetition rate. The 795 nm beam was then passed through a 50 : 50 beam splitter where the first half was directed towards a Fabry–Pérot Etalon (SLS Optics; spacing d = 10.3 μm, free spectral range [FSR] = 30.931 nm, effective finesse [F_{eff}] = 71.30 at 800 nm), which converted the incoming beam into a time-asymmetric picosecond visible pulse with an ~10–15 cm^{-1} full width half-maximum (FWHM). The other half of the beam was sent to an automated optical parametric amplification system. The broad bandwidth mid-IR beam was generated via the difference frequency generation process. The mid-IR beam has an FWHM ~200–250 cm^{-1}, in the range of 4000–1000 cm^{-1}. Both the 795 nm and mid-IR beams are focused to the sample stage with the IR beam aligned at an angle of 60° and the visible (795 nm) beam at an angle of 50° from the surface normal. When the incident IR beam is centered at 2900 cm^{-1}, the broadband SFG beam has a spot size of ~160–200 μm at an angle of 52° from the surface normal. The SFG signal is then collected with lenses, polarizer, spectrograph, and a detector.[16] The energies of the incident beams after the focusing lenses at air–liquid and air–solid interfaces are 9 μJ (IR) : 65 μJ (795 nm) and 7 μJ (IR) : 56 μJ (795 nm), respectively.

Beam Quality–Spot Sizes

The incident visible beam spot was measured using a Beamage series beam profiling camera (Gentec Electro-Optics, QC, Canada). The profile of the beam image was assessed using the "four-sigma ISO" where the beam widths are defined as an extent of a power density distribution in a cross-section of the beam based on the centered second order moments of the power density distribution. The IR spot size was measured using the knife-edge technique and the FWHM of the beam was determined to be ~100 μm.

Alignment

The spatial and temporal overlap of the beams was optimized using a gold thin film on a silicon wafer at PPP polarization when the IR beam was centered at 2900 cm^{-1}. Then, the IR spectrum of the polystyrene was taken for calibration of the *x*-axis. The SFG spectra from the ODT monolayers on gold were collected with PPP polarization combination at the resonant timing. The resonant timing was obtained when the delay of t = ~1.6 picoseconds was applied to suppress the SFG nonresonant signal from the gold surface. At the nonresonant timing (t = 0), the observed SFG signal is a combination of the signal from the interfacial molecules and the gold substrate, whereas, at the resonant timing, the asymmetric pulse shape of the 795 nm beam allows for the observation of the SFG signal only from the interfacial molecules. The peak profiles are shown as dips in the spectrum from a large nonresonant signal, and by suppressing the nonresonant response, the signal in the SFG spectrum appeared as peaks with the baseline close to zero.[25]

As a reference, the 100% ODT : 0% d_{37} ODT on the gold spectrum at the nonresonant timing was shown in the Supplemental Material as Fig. S1. The spectra were acquired for 60 s with one accumulation per second at 2900 cm^{-1} (C–H region) and 2200 cm^{-1} (C–D region). The spectra of EA monolayers were acquired at nonresonant timing for 9 min with one accumulation every 3 s. The SSP, PPP, and SPS polarization combinations spectra in the C–H region and only the SSP polarization combination spectra in the C–D region were collected. All raw spectra were corrected for the background.

Results and Discussion

The orientations of the terminal CH_3 group of the SAMs of ODT on gold and EA on the water were determined as a function of surface concentration. The S/N ratio for the symmetric stretch of the terminal CH_3 group was determined as a measure of the sensitivity of the SFG spectroscopy. The S/N ratio calculations are carried out before smoothing of the spectra. The dependence of the S/N ratio on the input power density of the visible beam was also determined using the spectra of 100% ODT : 0% d_{37} ODT and 100% EA : 0% d EA monolayers.

Air–Solid Interface: ODT/d_{37} ODT Self-Assembled Monolayers on Gold

The ODT–d_{37} ODT SAMs on gold were investigated to determine the orientation of the terminal methyl group since the surface concentration changes with concentration, especially at lower concentrations. Figure 1 shows the SFG spectra acquired with the PPP polarization combination in both C–H and C–D stretching regions taken at the resonant timing. The figure also includes pictures of the molecular structures of both ODT and deuterated ODT.

In the C–H stretching region, there are four peaks associated with the vibrational modes, ~2855 cm^{-1}, ~2880 cm^{-1}, ~2940 cm^{-1}, and ~2980 cm^{-1} assigned to

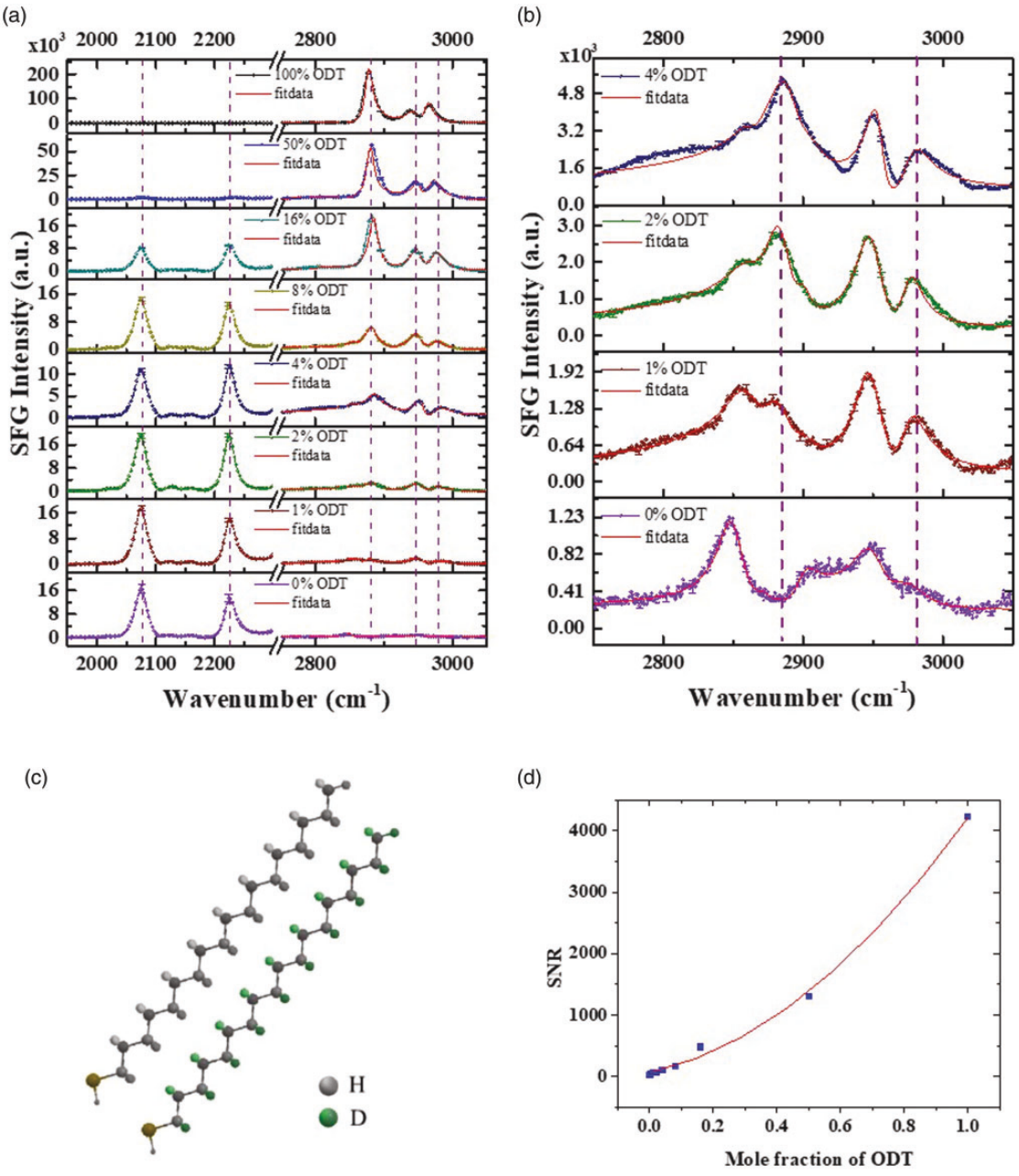

Figure 1. (a) Sum frequency generation spectra of self-assembled monolayers on the gold substrate prepared from various percentage solution between ODT and d_{37} ODT at the air–solid interface taken at PPP polarization combination in the C–H and C–D regions. (b) PPP SFG Spectra of 0%, 1%, 2%, and 4% ODT to show that the CH_3 SS peak at 2880 cm^{-1} and CH_3 AS peak at 2980 cm^{-1} from CH_3 group of ODT molecules. The red line in each spectrum in the C–H region corresponds to the fitted SFG spectrum. (c) Molecular structures of ODT and d_{37} ODT. (d) The plot of S/N ratio for CH_3 SS as a function of mole fraction of ODT with the quadratic fit (red line).

the methylene symmetric stretch (CH_2 SS),[26,27] methyl symmetric stretch (CH_3 SS),[23,26–30] methyl symmetric stretch split due to the Fermi resonance of the methyl bending vibration (CH_3 FR),[26,27,29,30] and the methyl antisymmetric stretch (CH_3 AS),[27,30] respectively. Due to the broadness of the spectral features in the range of 2880–2950 cm^{-1},[31] the methylene antisymmetric stretches and methylene Fermi resonances are not resolved in the SFG spectra. However, these vibrational peaks (resulting from methylene antisymmetric stretches and methylene Fermi resonances) were considered in the fitting of spectra. With the increasing percentage of the d_{37} ODT in the bulk

solution, the signal in the C–H region decreases due to a reduced number of ODT molecules against the deuterated counterpart. In the C–D stretching region, two peaks positioned at ~2225 cm^{-1} and ~2075 cm^{-1} are assigned to the CD_3 AS and CD_3 SS, respectively.[30,32–36]

Changes in Spectral Profile

At 100% ODT : 0% d_{37} ODT, a well-ordered self-assembled monolayer was obtained because the three vibrational modes visible in the C–H stretching region of the PPP spectrum originate solely from the terminal CH_3 group of the alkyl chain. Also, the SFG signal was also collected in the C–D region, and there were no observable peaks there. Next, the PPP spectrum collected from 50% ODT : 50% d_{37} ODT shows peaks from both the terminal CH_3 and CD_3 groups which indicated ordered and packed SAMs on the gold surface. The C–D peaks in the 50% ODT : 50% d_{37} ODT SFG spectrum have relatively low intensity compared to the C–H stretching region as shown in Fig. 1. Thus, a zoomed-in plot of the C–D region spectrum with the CD_3 group peaks is provided in Fig. S2 of the Supplemental Material. The 16% ODT : 84% d_{37} ODT still obtained a well-ordered ODT monolayer on gold because there is no considerable contribution from the methylene groups of the alkyl chain.

The transition from 16% ODT : 84% d_{37} ODT to 8% ODT : 92% d_{37} ODT has a substantial effect on the spectral profile of the PPP spectrum acquired in the C–H region. The CH_2 SS from the CH_2 groups in the C_{18} long chain become more noticeable than that in 100% ODT : 0% d_{37} ODT. The presence of the CH_2 SS in the SAMs is indicative of conformational disorder of ODT monolayers. Several studies have reported that the observation of the CH_2 group vibrational modes in the spectra was related to less ordered or loosely packed SAMs on a gold surface and the breaking of the trans-conformation.[28,32,37–43]

On the other hand, there is also a noticeable increase in the intensity of the C–D peaks when ~92% of the d_{37} ODT molecules are assembled on the gold surface. Next, additional SFG spectra were obtained for the 4% ODT : 96% d_{37} ODT, 2% ODT : 98% d_{37} ODT, 1% ODT : 99% d_{37} ODT, and 0% ODT : 100% d_{37} ODT, as shown in Fig. 1b. The PPP spectra obtained from 4%, 2%, and 1% of ODT molecules in the solutions have a similar spectra profile with CH_2 SS, CH_3 SS, CH_3 FR, and CH_3 AS vibrational modes from the long chain of the CH_2 groups and a terminal CH_3 group.

The SFG signal intensity is proportional to the square of the number density of the molecular groups. This relationship was supported by experimental data where the intensity of the CH_3 SS increased quadratically with mole fractions of the protonated ODT, as shown in Fig. S3. In addition, the source of peaks in the SFG spectrum of a self-assembled monolayer (SAM) prepared from a 0% ODT : 100% d_{37} ODT solution can be due to the chemical, isotopic, or substrate impurities. The chemical impurities have a lesser probability to adhere to the gold substrate compared to ODT molecules. However, since our system can detect protonated ODT in a SAM on gold from 1% ODT : 99% d_{37} ODT solution, with 1.8% chemical impurity as reported by the manufacturer, this impurity can still be a source of the methylene symmetric stretch peak present at the SFG spectrum of a SAM prepared from a 100% deuterated ODT solution. In addition, the CH vibrational bands in the SFG spectrum of the clean gold substrate are at a minimum. The peaks in the spectrum of the 0% ODT : 100% d_{37} ODT monolayer is also likely due to the 0.9% residual H isotopes. Therefore, it is possible that there are some molecules of d_{37}-ODT with incomplete deuteration, which could give rise to the CH_2 and CH vibrational bands (~2850 cm^{-1} and ~2910 cm^{-1}) in the 0% ODT spectrum. The ^{13}C APT NMR and IR spectra of bulk d_{37} ODT sample confirmed the presence of these residual CH and CH_2 groups in d_{37} ODT sample (Fig. S4). More importantly, the spectrum of the 1% ODT : 99% d_{37} ODT still has noticeable peaks arising from the vibrational mode of the terminal CH_3 group. The spectrum from the C–D region of the same sample (1% ODT and 99% d_{37} ODT) shows the CD_3 symmetric and CD_2 symmetric stretches where the peaks are positioned at ~2198 cm^{-1} and ~2019 cm^{-1}, respectively. The C–D spectra obtained from the self-assembled monolayers of different concentration ratios indicated the formation of ordered monolayers. The result obtained shows that the SFG spectroscopy can detect as low as 1% of ODT with 99% d_{37} ODT molecules on the gold surface at the air–monolayer interface. It is important to note here that the isotopic purity of the d_{37} ODT is 99.1% (CDN Isotopes, Inc., Pointe-Claire, Canada). However, chemical purity is ~98.2%. Therefore, its isotopic purity can limit the SFG studies at lower surface concentrations especially at ~0.9% other than the sensitivity of the SFG spectroscopy. This limitation can also be applied for the air–liquid interface system of an eicosanoic acid monolayer on water.

Orientation and Sensitivity Determination as a Function of Surface Concentration

To determine the SAM orientation, the PPP spectra in the C–H region were fitted using Eq. 1 (the fitting parameters are available in Tables S2–S4). The intensity ratio of the CH_3 SS and CH_3 AS was calculated for 100% ODT : 0% d_{37} ODT, 50% : 50%, 8% : 92%, 4% : 96%, 2% : 98%, and 1% : 99%, respectively, for the tilt angle analysis. In addition, the amplitude ratios between the CH_3 SS and CH_3 AS were calculated to estimate the distribution angle of different simulated tilt angle curves. The simulated curves with the calculated intensity and amplitude ratios to obtain the tilt angle and distribution angles are available in Fig. 2.

The details of the equations involved and the generation of simulated curves for the orientational analysis are

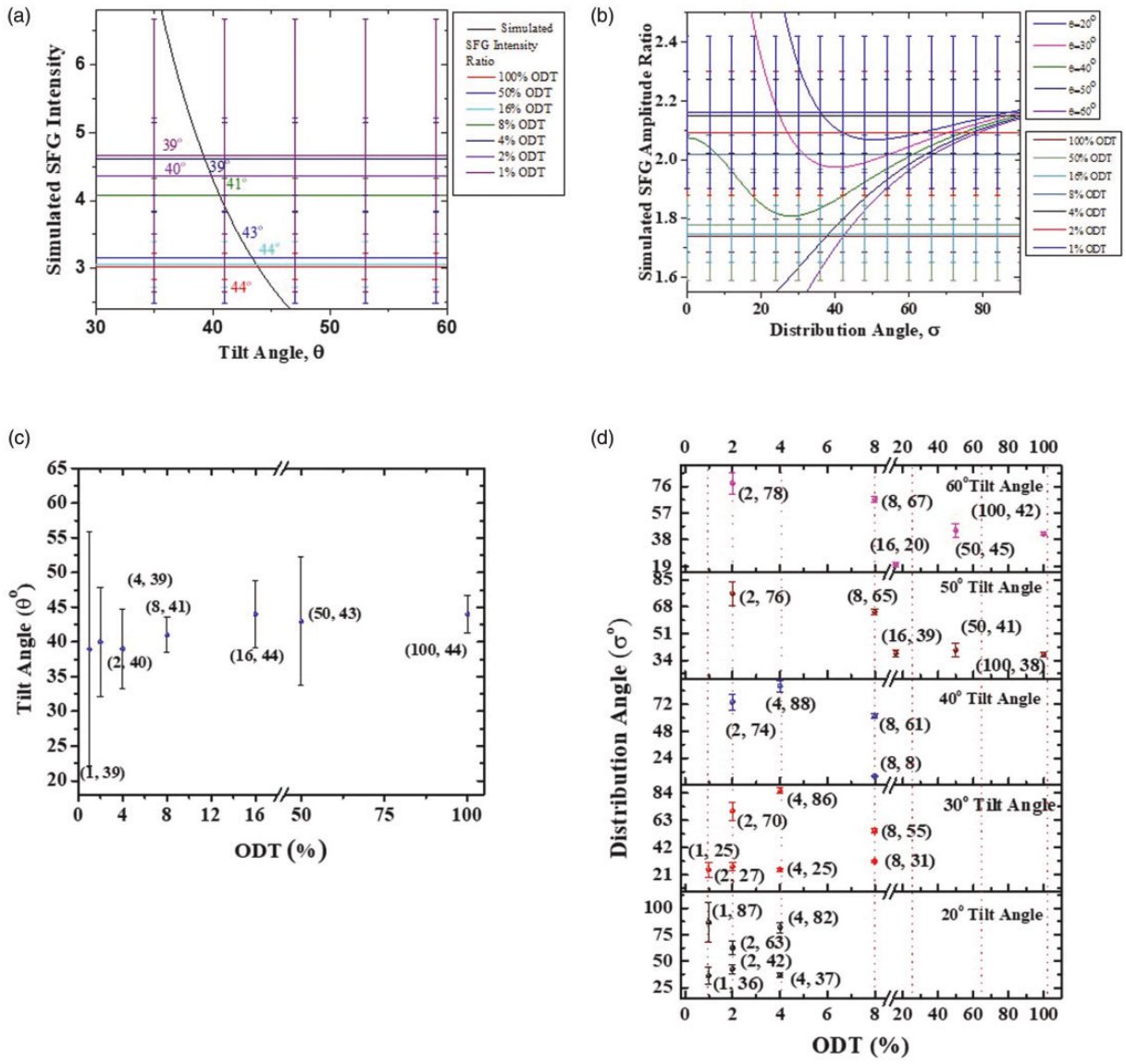

Figure 2. (a) Simulated curves of the SFG intensity ratios (CH_3 SS / CH_3 AS) at the PPP polarization combination as a function of tilt angle of the terminal methyl group, (b) simulated curves of the SFG amplitude ratios (CH3 SS/CH3 AS) at the PPP polarization combination as a function of the distribution angle, (c) the tilt angle of the terminal methyl group as a function of different concentration ratios, and (d) the distribution angle of the tilt angles as a function of different concentration ratios between the ODT and d_{37} ODT molecules.

available in our previous publications[14,15,17] and are also provided in the Supplemental Material. The orientational analysis is employed to the terminal CH_3 group of the ODT self-assembled monolayer on gold. A C_3V point group symmetry for the terminal CH_3 group was used to generate the simulated curves for the PPP polarization. The depolarization ratio used was 3.4[32,44,45] and the refractive indices of the air, gold metal, and the air–solid interface was estimated for the fixed visible frequency, mid-IR frequency, and sum frequency generation light.[46] The estimated tilt angles are within the reported values.[47–54] Overall, the tilt angles obtained for the CH_3 SS of the different concentration ratios are positioned closer to the surface normal. The long chain ODT and d_{37} ODT self-assembled monolayers adapt to an all-trans configuration.

There is no significant change in the tilt angles obtained from the fitting results of 100% ODT : 0% d_{37} ODT to 1% ODT : 99% d_{37} ODT. For example, the tilt angle obtained from the 1% ODT : 99% d_{37} ODT has a tilt angle of 39°. The noticeable error bar of the estimated tilt angle obtained from this concentration ratio could be due to the outcome of the fitting analysis of the 1% ODT : 99% d_{37} ODT PPP SFG spectrum. The fitting equation (Eq. 1) employed contains the term for nonresonant contribution as there is a possibility that the nonresonant response is not completely suppressed experimentally. Thus, the fitting

of the spectra is complicated due to the interference effects from the nonresonant signal and in turn will affect the tilt angle values obtained. The spectral profile variations at lower ODT concentrations could be due to the contribution from nonresonant response rather than a structural change in the monolayer. As discussed in a study by Patterson et al.,[55] nonresonant response should not be treated as a frequency independent amplitude. They further discuss that even though the nonresonant response is suppressed experimentally, spectral distortions can occur due to apodization of the resonant signal. These limitations can affect the overall fitting of the spectra and orientational analysis. However, the apodization effects arising from nonresonant signal suppression are consistent for relative comparisons between different ODT samples as carried out in this work.

Figure 2b also presents the distribution angles obtained for specific tilt angles at different concentration ratios. For example, the amplitude ratio obtained from the fitted spectra of a 100% ODT : 0% d_{37} ODT matched the 50° and 60° tilt angle simulated curves with relatively the same distribution angles of 38° and 42°, respectively. The width of the tilt angle value is slightly broader at 60° compared to 50°. A narrow distribution angle means the amplitude ratio matched a tilt angle simulated curve and the angle of deviation from that specific tilt angle is small. The values of the distribution angles were in the range of 8°–88°; however, some tilt angles, such as 20° and 30° especially for monolayers at lower concentration ratios of ODT, have two solutions for the distribution angles. Another example is the solution for the 1% ODT : 99% d_{37} ODT spectrum obtained a distribution angle value of 87° at 20° tilt angle; this broad distribution angle means that there is a large angle of deviation from the tilt angle of 20°.

Moreover, the S/N ratio was also determined for all the spectra obtained in the C–H stretching region as a measure of the sensitivity of the SFG spectrometer. Signal-to-noise ratio increases as the concentration of the protonated ODT molecules increases in the solution mixture used to prepare SAMs on gold as shown in Fig. 1d. The S/N ratio scale changes quadratically with the mole fraction of protonated molecules because the noise is small and almost constant at different mole fractions, and the S/N ratio is proportional to the signal intensity which is also quadratically dependent on the number of CH_3 groups. To calculate the S/N ratio, the SFG intensity of the CH_3 SS vibrational mode at ~2875 cm^{-1} was divided by the standard deviation (SD) of the baseline noise estimated from 3200 cm^{-1} to 3250 cm^{-1}. This region was selected because there are no vibrational resonances present and the noise is due to the dark current (thermally generated noise of the charge-coupled device [CCD]) and scattering of any unwanted beams. Figure S5 shows the baseline noise for the spectra from monolayers of ODT : d_{37} ODT with different concentration ratios. Moreover, S/N ratio was determined to be ~60 for the 1% ODT : 99% d_{37} ODT monolayer.

Air–Liquid Interface: EA/d EA Monolayers on Water

To determine the sensitivity of the SFG system, a monolayer of EA and deuterated EA on water was prepared with different concentration ratios. The SFG spectra were acquired at SSP, PPP, and SPS polarizations for the orientation analysis and peak assignments.

Two types of deuterated EAs were selected to test the chemical sensitivity of the instrument at the air–liquid interface with changing the percent by volume between the protonated and deuterated EAs. The first experiment used a d_3 EA with only its terminal CH_3 group deuterated; the spectra including the picture of the EA molecular structures are provided in Fig. S6.

The spectrum in the CH spectrum has contributions from the terminal CH_3 group of the protonated EA, the CH_2 groups of the EA, and the d_3 EA carbon chains. To reduce the contribution of the CH_2 SS vibrational mode from the CH_2 groups of both the protonated and d_3 deuterated EAs, a molecule (d_{39} EA) with no C–H groups was also used in a similar experiment. Figure 3a shows the SSP SFG spectra collected at both C–H and C–D regions for the samples with different percentages between the protonated EA and the d_{39} EA. The SSP spectrum of the EA on water has two main peaks in the C–H stretching region positioned at ~2875 cm^{-1} and ~2950 cm^{-1}, which are assigned to CH_3 SS and CH_3 FR,[37,56–59] respectively. The shoulder peak at 2850 cm^{-1} is assigned to the CH_2 SS.[37,58,59] Even though the methylene antisymmetric stretches and methylene Fermi resonances were not clearly resolved due to the broadness of the spectral features from 2880–2950 cm^{-1},[31] we still considered these peaks in the fitting of the spectra. In the C–D region, three peaks are observed at ~2070 cm^{-1}, ~2130 cm^{-1}, and ~2220 cm^{-1} and are assigned to the CD_3 SS, CD_3 FR, and CD_3 AS, respectively.[32,60–63]

Changes in Spectral Profile

In the C–H stretching region, the SSP spectrum of 100% EA : 0% d_{39} EA on water has three peaks (CH_2 SS, CH_3 SS, and CH_3 FR positioned at ~2850 cm^{-1}, ~2875 cm^{-1}, and ~2940 cm^{-1}, respectively). The 50% EA : 50% d_{39} EA spectrum also shows the same vibrational peaks. Meanwhile, the spectra of 16% EA : 84% d_{39} EA, 2% EA : 98% d_{39} EA, and 1% EA : 99% d_{39} EA have only CH_3 SS, and CH_3 FR vibrational modes and the CH_2 SS peak is not evident in these spectra. Figure 3b shows a zoomed-in spectrum for the 2% EA, 1% EA, and 0% EA samples in the CH region for clarity. The intensity of CH_3 SS is plotted as a function of mole fraction of the EA (Fig. S7); as expected, the plot shows the intensity of CH_3 SS increases quadratically as the mole fraction of

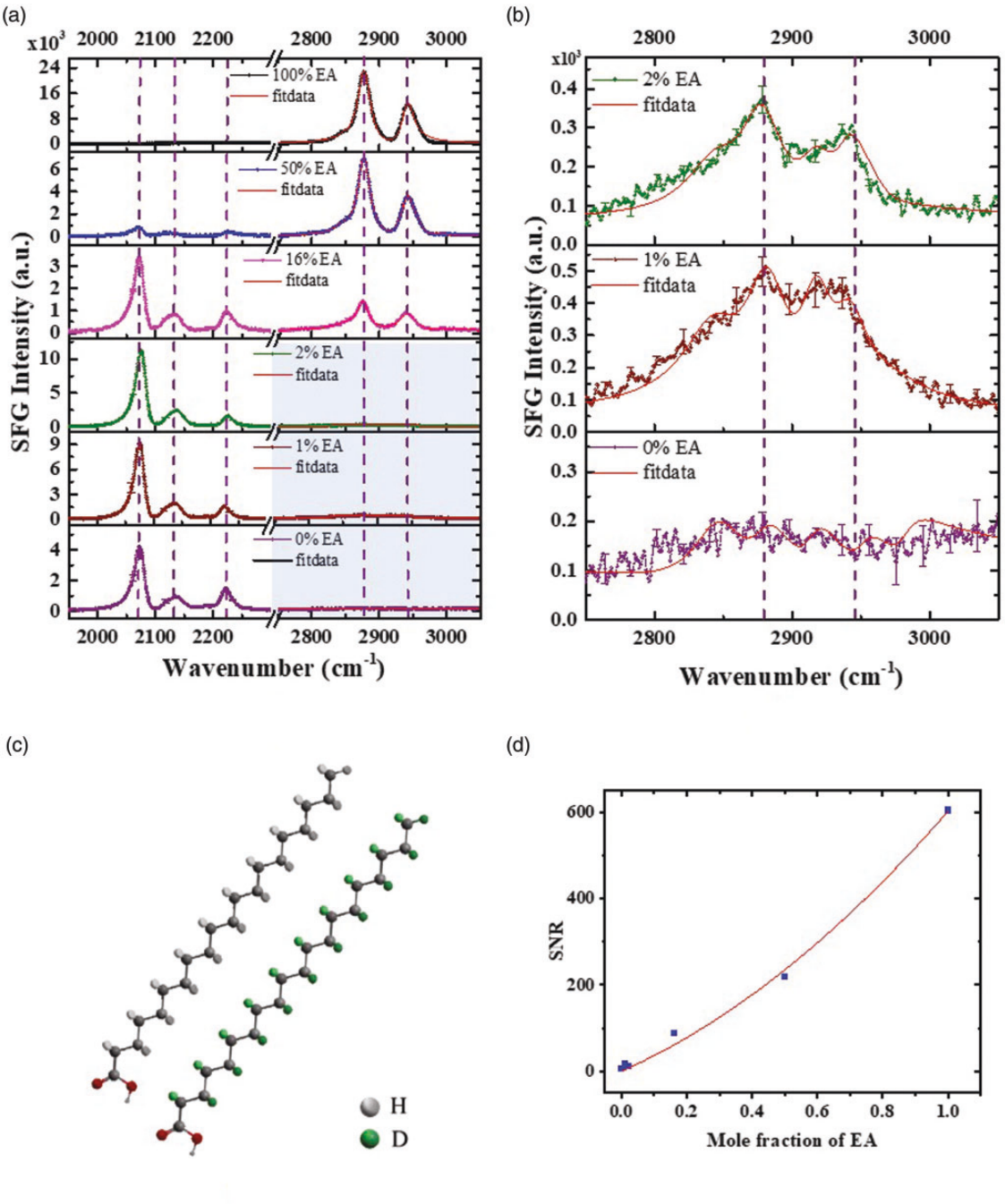

Figure 3. Sum frequency generation spectra of self-assembled monolayers of EA and d_{39} EA on water at the air–liquid interface taken at the SSP polarization combination in the C–H and C–D regions, (b) SSP SFG spectra plotted only for 0%, 1%, and 2% EA in the CH region for a clearer view, (c) molecular structures of the EA acid and d_{39} EA, and (d) a plot of the S/N ratio for the CH_3 SS as a function of mole fraction of EA with a quadratic fit (red line).

the EA increases. In addition, the 2% EA : 98% d_{39} EA and 1% EA : 99% d_{39} EA monolayers were prepared on deuterium oxide (D_2O) to obtain clear visibility of the peaks in the C–H region with less interference from the broad H_2O vibrational band (Fig. S8). In addition to the observed CH_3 SS and CH_3 FR vibrational modes in the spectra of 2% and 1% EA on H_2O, the CH_3 AS at 2970 cm^{-1} was also evident in the spectra of the 2% and 1% EA on D_2O.

In the C–D stretching region, the SSP spectrum of the 0% EA : 100% d_{39} EA, in Fig. 3a, consists of three peaks at ~2070 cm^{-1}, ~2130 cm^{-1}, and ~2220 cm^{-1} assigned to the CD_3 SS, CD_3 FR, and CD_3 AS, respectively. These three peaks are also observed in the SSP spectra of 50%

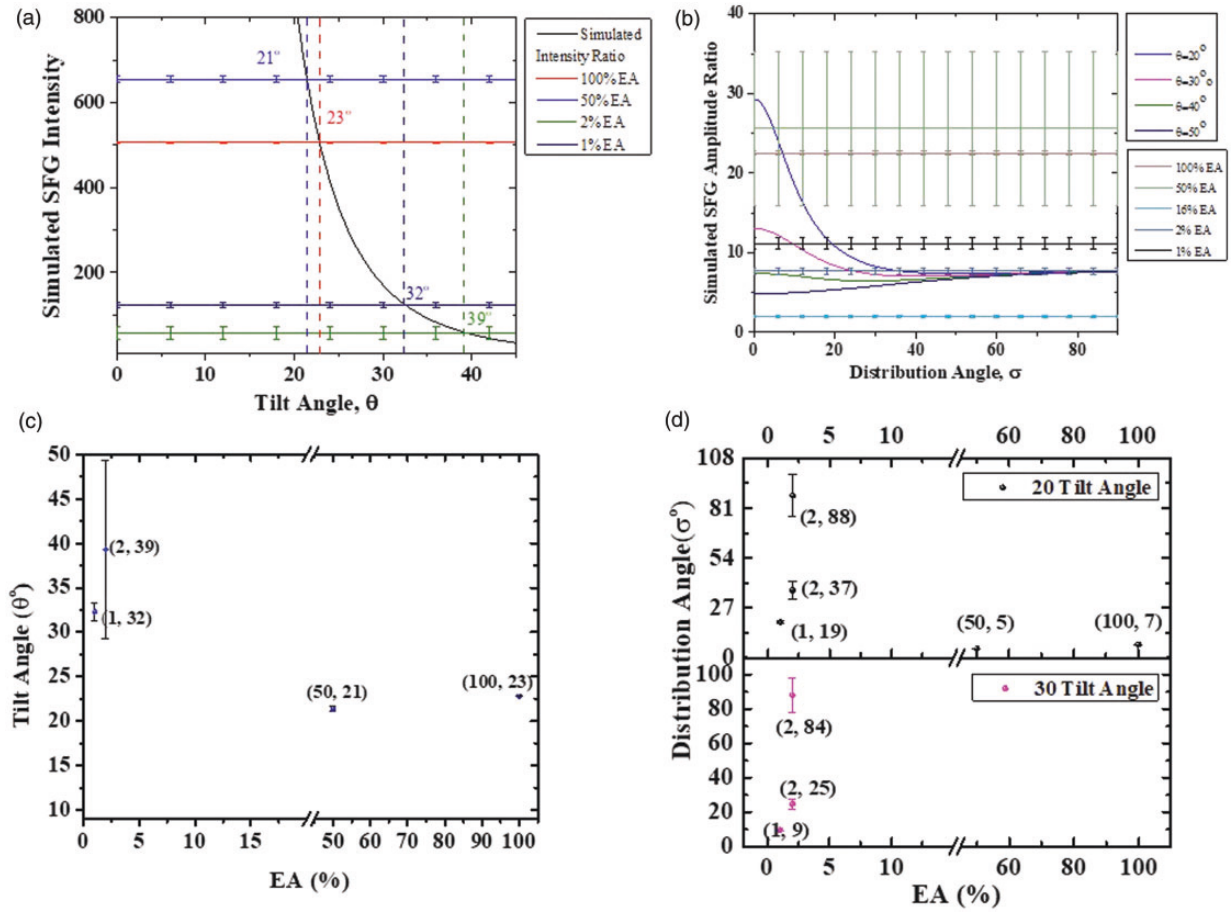

Figure 4. (a) Simulated curves of the SFG intensity ratios of the CH_3 SS (SSP/SPS) as a function of tilt angle of the terminal methyl group, (b) simulated curves of the SFG amplitude ratios of the CH3 SS (SSP/SPS) as a function of the distribution angle, (c) the tilt angle of the terminal methyl group as a function of different concentration ratios, and (d) distribution angle of the tilt angles as a function of different concentration ratios between the EA and d_{39} EA molecules.

EA : 50% d_{39} EA, 16% EA : 84% d_{39} EA, 2% EA : 98% d_{39} EA, and 1% EA : 99% d_{39} EA. Moreover, in the SSP spectrum of the 50% EA : 50% d_{39} EA, the C–D vibrational modes are not well-defined as shown in the graph because the C–H signal is relatively higher compared to the C–D signal. Therefore, a zoomed-in spectrum available in Fig. S9 of the Supplemental Material shows the CD_3 SS, CD_3 FR, and CD_3 AS vibrational modes. The spectra obtained in both the C–H and C–D regions for the 100% EA : 0% d_{39} EA correspond to the well-ordered monolayer.[37,38,59,64] With the 50% EA : 50% d_{39} EA, the presence of the CH_2 SS vibrational mode is indicative of conformational disorder of the monolayers. As explained earlier, only the CD_3 vibrational modes are observed in the C–D region. At 16% EA : 84% d_{39} EA, the SSP spectrum obtained from the C–H region has only two peaks that represent an ordered monolayer. Then, at 2% EA : 98% d_{39} EA, the C–H peaks in the C–H region are lower in intensity but still indicative of a well-ordered monolayer. Lastly, the 0% EA : 100% d_{39} EA SSP spectrum obtained from the C–H region shows that there are no C–H peaks visible in the C–H region.

Orientation and Sensitivity Determination as a Function of Surface Concentration

For the orientation analysis, the spectra obtained in the C–H stretching region with SSP, PPP, and SPS polarizations were fit using Eq. 1. In this paper, the amplitude and intensity ratios between the SSP and SPS polarizations were selected to estimate the tilt angle values and distribution angles as the concentration ratios are varied. The fitted spectra of the EA : d_{39} EA monolayers on water are available in the Supplemental Material (Fig. S10) and the fitting results are provided in the Supplemental Material as Tables S5–S10. Figures 4a and b show the simulated curves for the determination of the tilt and distribution angles. Figures 4c and d show plots of the tilt and distribution angles as a function of varying concentration ratios between the EA and d_{39} EA molecules.

After fitting the spectra and calculating both the amplitude and intensity ratios, the 16% EA with 84% of the d_{39} EA on the water surface did not provide a solution to obtain estimated values for both the tilt and distribution

angles of the CH_3 SS vibrational mode. As mentioned earlier, the ratios were obtained from the SSP and SPS polarization combinations. The tilt angle values obtained are within or less than the reported values for a terminal CH_3 group of a long chain compound.[47,48,51,65–67] The tilt angles at 1% EA : 99% d_{39} EA and 2% EA : 98% d_{39} EA have larger error bars compared to the other concentration ratios because of the relatively lower SFG signal compared to the EA formed with higher surface coverage. The low signal will, in turn, affect the reliability of the fitting, results, and the ratios needed to estimate the tilt and distribution angles. In Fig. 4b, the distribution angles for different concentration ratios were determined for 20° and 30° tilt angles. For the 100% EA : 0% d_{39} EA as an example, the fitting results obtained a ~7° distribution angle for a 20° tilt angle. The value had a relatively narrower width for the distribution angle, which shows a smaller deviation from the average tilt angle value as represented by the simulated curve. The solution of the distribution angle could not be estimated for a tilt angle of 30° because the ratio from the fitted data does not intersect the 30° simulated curve. The values plotted for the 2% EA : 98% d_{39} EA show relatively broader distribution angles which slightly decreased with the increasing tilt angle.

The orientation analysis at lower concentrations of protonated long chain molecules can be beneficial not only for the subsequent formation of self-assembled monolayers but also on any important interfacial chemical systems. Examples include studying the conformation of peptides in different environments.[68,69]

The S/N ratio was also determined for the spectra of the EA : d_{39} EA obtained in the C–H stretching region (Fig. 3a) as a measure of the sensitivity of the SFG spectroscopy at the air–liquid interface. The S/N ratio increases with the concentration of the protonated EA molecules in the solution mixture used to prepare the monolayer on the water surface as shown in Fig. 3d. The S/N ratio was determined to be ~18 for 1% EA : 99% d_{39} EA at the air–liquid interface using the same method applied in the ODT monolayer system.

The ability to detect signal and perform orientation analyses at lower concentrations at both the air–solid and air–liquid interfaces demonstrates the improved sensitivity of the SFG spectroscopy. Well-optimized SFG photon detection could be one possible reason for the observed improved sensitivity and S/N ratio. The detection side contains: (1) 1 : 1 telescopic lens system which allows better collection of the SFG signal generated at the sample surface; (2) custom-requested spectrograph with anti-reflective coated gratings optimized for the SFG light; and (3) a back-illuminated CCD that has deep depletion with fringe suppression capabilities and a 92% quantum efficiency when the SFG beam is collected at an IR center of 2900 cm^{-1}. To further investigate the sensitivity of the system, the next section considers other factors such as power density of incident beams that can affect the SFG intensity.

Sum Frequency Generation Intensity and Signal-to-Noise Ratio as a Function of the Power Density of Incident Beams

The intensity of the SFG signal depends on several experimental factors such as the experimental geometry of the setup, the angles of the incident beams, incident beam powers, and the detection system. We focus on the dependency of the SFG intensity on the incident beam power. First, we determined the energy density of the 795 nm beam at the sample stage. Figure S11 in the Supplemental Material shows the beam spots captured using the beam profiling camera with the Gaussian fitted curves along the major and minor axes of the beam spots. Two different 795 nm beam focusing lens positions were used for the analysis at the air–solid and air–liquid interfaces. Both beam spots had an elliptical shape, because of their non-normal incidence. The diameters of the major axes, minor axes, the effective diameters, and the area of the beam spots are provided in Table S11 containing four different values for the diameter obtained from the four various beam width definitions. After the systematic evaluation of the beam spot size, the power densities of both beam spots were calculated. Observation of the SFG signal with acceptable S/N ratio at low surface concentrations could be a result of the higher incident 795 nm power density. To evaluate this concept further, the SFG spectra of both the 100% ODT : 0% d_{37}ODT and 100% EA : 0% d EA were collected at different incident beam power densities. The visible beam power density was varied by adjusting the set of attenuating optics. To avoid localized surface heating and evaporation of the liquid at the interface, a slightly defocused visible beam was used for the 100% EA : 0% d EA system. Figure 5a shows the PPP polarized fitted SFG spectra of the 100% ODT : 0% d_{37}ODT at different 795 nm incident power densities. As expected, the intensity of the signal reduces with the power of the 795 nm beam. The fitted SFG intensity of the CH_3 SS increases quadratically as the power density of the incident visible beam increases. In addition, the calculated S/N ratio values for the CH_3 SS vibrational mode were found to show quadratic dependence to the changes incurred by the power density of the visible beam at the sample surface (Fig. 5c). This statement becomes more feasible with small or almost negligible changes in the noise as a function of power density that can affect the S/N ratio calculations. More importantly, even at a low power density, good S/N ratio value was obtained from the SFG spectrum.

For the 100% EA : 0% d EA system, the fitted intensity and the calculated S/N ratio for the CH_3 SS increase with the power density of the incident visible beam as shown in Fig. 5b and d. It is important to note here that at the

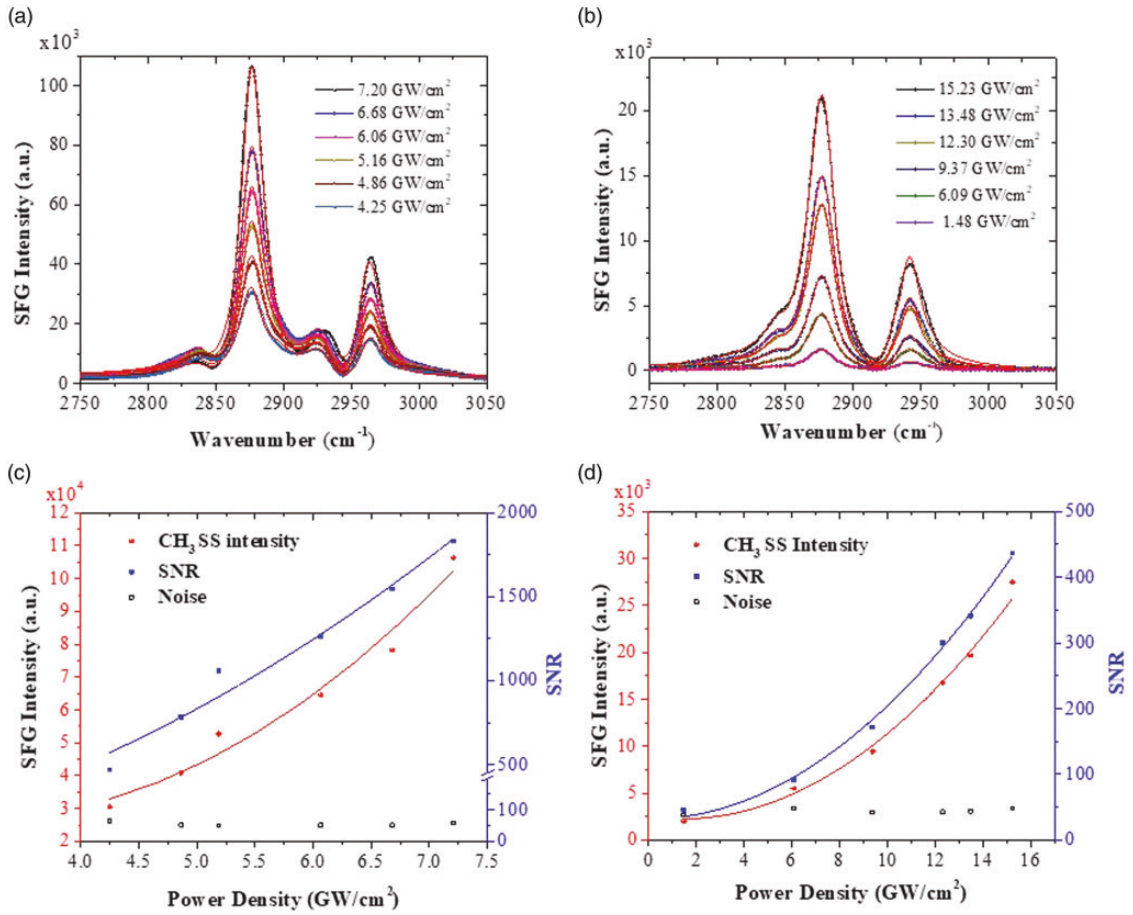

Figure 5. The SFG spectra as a function of the power density of the incident visible beam. (a) The PPP spectra with the corresponding fit (red lines) of the 100% ODT : 0% d_{39}ODT monolayer on gold. (b) SSP spectra of the 100% EA : 0% d EA monolayer on water. The intensity of the CH_3 SS (red dots), S/N ratio (blue squares), and baseline noise (open squares) as a function of the power density of the visible beam of (c) 100% ODT : 0% d_{39}ODT monolayer on gold and (d) and 100% EA : 0% d EA monolayer on water. The SFG intensity is plotted with a quadratic fit (red line) and S/N ratio with a quadratic fit (blue line).

air–liquid interface, since the incident visible beam spot size was adjusted and larger, a higher power (higher power density) was applied to the sample surface to obtain a comparable S/N ratio to that of the air–solid interface. As noted, the increase in the signal strength associated with the power density resulted in a quadratic increase in the S/N ratio with the value at the lowest power density being an outlier. Again, the fitted SFG intensity of the CH_3 SS increases as the power density of the incident visible beam increases.

Conclusion

The orientation of the methyl group of the self-assembled monolayers of ODT on gold and EA on water was determined as a function of the surface concentration under ambient conditions. The orientational analysis of the CH_3 SS from the terminal CH_3 group for the monolayers of the concentration ratios as low as 1% protonated molecules in the presence of 99% deuterated molecules shows that the tilt angles obtained are reliable and close to the previously reported values of well-ordered monolayers. The ability to determine the orientation at low surface concentrations highlighted the improved sensitivity of the SFG spectroscopy. A S/N ratio of ~60 was achieved for 1% ODT : 99% d_{39} ODT. Moreover, at the air–liquid interface, a S/N ratio of ~18 was achieved at the 1% EA : 99% d_{39} EA (0.15 molecules/nm^2). Considering the quadratic dependence of S/N ratio on surface concentration, an acceptable S/N ratio value of 3 can be achieved when the ODT and EA concentrations are 0.2% and 0.9%, respectively. Even though the ODT monolayers on the gold yields a better S/N ratio compared to that of the EA monolayers on water, the large error bars were obtained in the ODT tilt angle calculations. When compared to EA, more acceptable error bars were acquired for each concentration and could be a result of: (1) using one versus two polarization methods for tilt angle calculations at different interfaces; and (2) due to the interference effects of nonresonant response in ODT on the gold system. Another probable cause of deviation

could be a result of fitting and calculation of uncertainties with a 95% confidence level. Overall, the orientational analysis of CH_3 SS vibrational mode was performed at low concentrations of protonated molecules due to increased S/N ratio. In support, the increased S/N ratio on varying incident power density of the visible beam was also experimentally demonstrated. Finally, the advantage of having the ability to determine the orientation of interfacial molecules at low concentrations with improved sensitivity in the SFG spectroscopic system will allow, for example, detecting and understanding the effects of smaller concentrations of amino acids on a lipid monolayer or interactions of peptides in a different chemical environment.

Acknowledgments

The authors thank Dr. JoonHee Jang for his helpful assistance and discussions. The authors are also grateful to Ahmed Aboelenen and Prof. Michael Jensen for the IR characterization of the deuterated samples used in this manuscript. In addition, the authors thank the Nanoscale and Quantum Phenomena Institute and Condensed Matter and Surface Science for their additional financial support.

Conflict of Interest

There are no conflicts to declare.

Funding

The current work has been supported by the start-up fund provided by Ohio University. This work was supported by the National Science Foundation under Grant No. CHE-0947031 for the acquisition of the femtosecond laser. Uvinduni Premadasa was partially supported by the National Science Foundation under Grant No. CBET-1705817.

ORCID iD

Katherine Leslee A. Cimatu https://orcid.org/0000-0002-4216-9715

Supplemental Material

All supplemental material mentioned in the text, consisting of materials, fitted spectra of d_{39} EA, fitting parameters, and details on spot size measurements, is available in the online version of the journal.

References

1. F. Vidal, B. Busson, A. Tadjeddine. "Probing Electronic and Vibrational Properties at the Electrochemical Interface Using SFG Spectroscopy: Methanol Electro-Oxidation on Pt(110)". Chem. Phys. Lett. 2005. 403(4): 324–328.
2. L. Fu, J. Liu, E.C. Yan. "Chiral Sum Frequency Generation Spectroscopy for Characterizing Protein Secondary Structures at Interfaces". J. Am. Chem. Soc. 2011. 133(21): 8094–8097.
3. A.L. Barnette, L.C. Bradley, B.D. Veres, et al. "Selective Detection of Crystalline Cellulose in Plant Cell Walls with Sum Frequency Generation (SFG) Vibration Spectroscopy". Biomacromol. 2011. 12(7): 2434–2439.
4. C. Weeraman, A.K. Yatawara, A.N. Bordenyuk, et al. "Effect of Nanoscale Geometry on Molecular Conformation: Vibrational Sum Frequency Generation of Alkanethiols on Gold Nanoparticles". J. Am. Chem. Soc. 2006. 128(44): 14244–14245.
5. S. Baldelli. "Probing Electric Fields at the Ionic Liquid−Electrode Interface Using Sum Frequency Generation Spectroscopy and Electrochemistry". J. Phys. Chem. B. 2005. 109(27): 13049–13051.
6. C. Aliaga, S. Baldelli. "Sum Frequency Generation Spectroscopy and Double-Layer Capacitance Studies of the 1-Butyl-3-Methylimidazolium Dicyanamide−Platinum Interface". J. Phys. Chem. B. 2006. 110(37): 18481–18491.
7. B.A. Rosen, J.L. Hahn, P. Mukherjee, et al. "In situ Spectroscopic Examination of a Low Overpotential Pathway for Carbon Dioxide Conversion to Carbon Monoxide". J. Phys. Chem. C. 2012. 116(29): 15307–15312.
8. S. Ye, A. Kathiravan, H. Hayashi, et al. "Role of Adsorption Structures of Zn–Porphyrin on TiO_2 in Dye-Sensitized Solar Cells Studied by Sum Frequency Generation Vibrational Spectroscopy and Ultrafast Spectroscopy". J. Phys. Chem. C. 2013. 117(12): 6066–6080.
9. Y.R. Shen. "Surface Properties Probed by Second Harmonic and Sum Frequency Generation". Nature. 1989. 337(6207): 519–525.
10. D. Zhang, J. Gutow, K.B. Eisenthal. "Vibrational Spectra, Orientations, and Phase Transitions in Long Chain Amphiphiles at the Air/Water Interface: Probing the Head and Tail Groups by Sum Frequency Generation". J. Phys. Chem. 1994. 98(51): 13729–13734.
11. S. Gopalakrishnan, P. Jungwirth, D.J. Tobias, et al. "Air-Liquid Interfaces of Aqueous Solutions Containing Ammonium and Sulfate: Spectroscopic and Molecular Dynamics Studies". J. Phys. Chem. B. 2005. 109(18): 8861–8872.
12. G. Ma, H.C. Allen. "DPPC Langmuir. Monolayer at the Air-Water Interface: Probing the Tail and Head Groups by Vibrational Sum Frequency Generation Spectroscopy". Langmuir. 2006. 22(12): 5341–5349.
13. P.B. Miranda, Y.R. Shen. "Liquid Interfaces: A Study by Sum Frequency Vibrational Spectroscopy". J. Phys. Chem. B. 1999. 103(17): 3292–3307.
14. S.C. Chan, J.H. Jang, K.L.A. Cimatu. "Orientational Analysis of Interfacial Molecular Groups of 2-Methoxyethyl Methacrylate Monomer Using Femtosecond Sum Frequency Generation Spectroscopy". J. Phys. Chem. C. 2016. 120(51): 29358–29373.
15. U.I. Premadasa, N.M. Adhikari, S. Baral, et al. "Conformational Changes of Methacrylate-Based Monomers at the Air–Liquid Interface Due to Bulky Substituents". J. Phys. Chem. C. 2017. 121(31): 16888–16902.
16. K.L.A. Cimatu, S.C. Chan, J.H. Jang, et al. "Preferential Organization of Methacrylate Monomers and Polymer Thin Films at the Air Interface Using Femtosecond Sum Frequency Generation Spectroscopy". J. Phys. Chem. C. 2015. 119(45): 25327–25339.
17. N.M. Adhikari, U.I. Premadasa, K.L.A. Cimatu. "Sum Frequency Generation Vibrational Spectroscopy of Methacrylate-Based Functional Monomers at the Hydrophilic Solid-Liquid Interface". Phys. Chem. Chem. Phys. 2017. 19(32): 21818–21828.
18. A.P. Boughton, P. Yang, V.M. Tesmer, et al. "Heterotrimeric G Protein $\beta 1\gamma 2$ Subunits Change Orientation Upon Complex Formation with G Protein-Coupled Receptor Kinase 2 (GRK2) on a Model Membrane". Proc. Natl. Acad. Sci. U.S.A. 2011. 108(37): E667–E673.
19. C.-y. Wang, H. Groenzin, M.J. Shultz. "Surface Characterization of Nanoscale TiO_2 Film by Sum Frequency Generation Using Methanol as a Molecular Probe". J. Phys. Chem. B. 2004. 108(1): 265–272.
20. C.L. Anfuso, D. Xiao, A.M. Ricks, et al. "Orientation of a Series of CO_2 Reduction Catalysts on Single Crystal TiO_2 Probed by Phase-Sensitive Vibrational Sum Frequency Generation Spectroscopy (PS-VSFG)". J. Phys. Chem. C. 2012. 116(45): 24107–24114.
21. A.K. Yatawara, G. Tiruchinapally, A.N. Bordenyuk, et al. "Carbohydrate Surface Attachment Characterized by Sum

Frequency Generation Spectroscopy". Langmuir. 2009. 25(4): 1901–1904.
22. R. Maoz, J. Sagiv, D. Degenhardt, et al. "Hydrogen-Bonded Multilayers of Self-Assembling Silanes: Structure Elucidation by Combined Fourier Transform Infra-Red Spectroscopy and X-ray Scattering Techniques". Supramol. Sci. 1995. 2(1): 9–24.
23. D. Verreault, V. Kurz, C. Howell, et al. "Sample Cells for Probing Solid/Liquid Interfaces with Broadband Sum Frequency Generation Spectroscopy". Rev. Sci. Instrum. 2010. 81(6): 063111.
24. I.V. Stiopkin, H.D. Jayathilake, A.N. Bordenyuk, et al. "Heterodyne Detected Vibrational Sum Frequency Generation Spectroscopy". J. Am. Chem. Soc. 2008. 130(7): 2271–2275.
25. A. Lagutchev, S.A. Hambir, D.D. Dlott. "Nonresonant Background Suppression in Broadband Vibrational Sum Frequency Generation Spectroscopy". J. Phys. Chem. C. 2007. 111(37): 13645–13647.
26. A.D. Quast, N.C. Wilde, S.S. Matthews, et al. "Improved Assignment of Vibrational Modes in Sum Frequency Spectra in the CH Stretch Region for Surface-bound C18 Alkylsilanes". Vib. Spectrosc. 2012. 61: 17–24.
27. L.J. Richter, T.P. Petralli-Mallow, J.C. Stephenson. "Vibrationally Resolved Sum Frequency Generation with Broad Bandwidth Infrared Pulses". Opt. Lett. 1998. 23(20): 1594–1596.
28. A.M. Ge, Q.L. Peng, L. Qiao, et al. "Molecular Orientation of Organic Thin Films on Dielectric Solid Substrates: A Phase-Sensitive Vibrational SFG Study". Phys. Chem. Chem. Phys. 2015. 17(27): 18072–18078.
29. C.D. Bain, P.B. Davies, T.H. Ong, et al. "Quantitative Analysis of Monolayer Composition by Sum Frequency Vibrational Spectroscopy". Langmuir. 1991. 7(8): 1563–1566.
30. G. Ma, H.C. Allen. "Surface Studies of Aqueous Methanol Solutions by Vibrational Broad Bandwidth Sum Frequency Generation Spectroscopy". J. Phys. Chem. B. 2003. 107(26): 6343–6349.
31. S.K. Das, S. Sengupta, L. Velarde. "Interfacial Surfactant Ordering in Thin Films of SDS-Encapsulated Single-Walled Carbon Nanotubes". J. Phys. Chem. Lett. 2016. 7(2): 320–326.
32. E. Tyrode, J. Hedberg. "A Comparative Study of the CD and CH Stretching Spectral Regions of Typical Surfactants Systems Using VSFS: Orientation Analysis of the Terminal CH_3 and CD_3 Groups". J. Phys. Chem. C. 2012. 116(1): 1080–1091.
33. M.L. Clarke, Z. Chen. "Polymer Surface Reorientation After Protein Adsorption". Langmuir. 2006. 22(21): 8627–8630.
34. T. Iwahashi, T. Ishiyama, Y. Sakai, et al. "Liquid/Liquid Interface Layering of 1-Butanol and [bmim] PF 6 Ionic Liquid: A Nonlinear Vibrational Spectroscopy and Molecular Dynamics Simulation Study". Phys. Chem. Chem. Phys. 2015. 17(38): 24587–24597.
35. G. Ma, H.C. Allen. "Real-Time Investigation of Lung Surfactant Respreading with Surface Vibrational Spectroscopy". Langmuir. 2006. 22(26): 11267–11274.
36. K. Tian, H. Li, S. Ye. "Methanol Perturbing Modeling Cell Membranes Investigated Using Linear and Nonlinear Vibrational Spectroscopy". Chinese J. Chem. Phys. 2013. 26(1): 27–34.
37. A.G. Lambert, P.B. Davies, D. Neivandt. "Implementing the Theory of Sum Frequency Generation Vibrational Spectroscopy: A Tutorial Review". Appl. Spectrosc. Rev. 2005. 40(2): 103–145.
38. N. Takeshita, M. Okuno, T.-a. Ishibashi. "Molecular Conformation of DPPC Phospholipid Langmuir. and Langmuir–Blodgett Monolayers Studied by Heterodyne-Detected Vibrational Sum Frequency Generation Spectroscopy". Phys. Chem. Chem. Phys. 2017. 19: 2060–2066.
39. Z. Avazbaeva, W. Sung, J. Lee, et al. "Origin of the Instability of Octadecylamine Langmuir Monolayer at Low pH". Langmuir. 2015. 31(51): 13753–13758.
40. M. Schleeger, Y. Nagata, M. Bonn. "Quantifying Surfactant Alkyl Chain Orientation and Conformational Order from Sum Frequency Generation Spectra of CH Modes at the Surfactant–Water Interface". J. Phys. Chem. Lett. 2014. 5(21): 3737–3741.
41. C. Meltzer, J. Paul, H. Dietrich, et al. "Indentation and Self-Healing Mechanisms of a Self-Assembled Monolayer A Combined Experimental and Modeling Study". J. Am. Chem. Soc. 2014. 136(30): 10718–10727.
42. J. Weber, T. Balgar, E. Hasselbrink. "Conformational Disorder in Alkylsiloxane Monolayers at Elevated Temperatures". J. Chem. Phys. 2013. 139(24): 244902.
43. B.W. Ewers, J.D. Batteas. "Molecular Dynamics Simulations of Alkylsilane Monolayers on Silica Nanoasperities: Impact of Surface Curvature on Monolayer Structure and Pathways for Energy Dissipation in Tribological Contacts". J. Phys. Chem. C. 2012. 116(48): 25165–25177.
44. H.-F. Wang, W. Gan, R. Lu, et al. "Quantitative Spectral and Orientational Analysis in Surface Sum Frequency Generation Vibrational Spectroscopy (SFG-VS)". Int. Rev. Phys. Chem. 2005. 24(2): 191–256.
45. D.A. Beattie, R. Fraenkel, S.A. Winget, et al. "Sum-Frequency Spectroscopy of a Monolayer of Zinc Arachidate at the Solid—Solid Interface". J. Phys. Chem. B. 2006. 110(5): 2278–2292.
46. G.M. Hale, M.R. Querry. "Refractive Index Database". http://refractiveindex.info [accessed 26 April 2018].
47. R. Arnold, A. Terfort, C. Wöll. "Determination of Molecular Orientation in Self-Assembled Monolayers Using IR Absorption Intensities: The Importance of Grinding Effects". Langmuir. 2001. 17(16): 4980–4989.
48. R.D. Mountain, J.B. Hubbard, C.W. Meuse, et al. "Molecular Dynamics Study of Partial Monolayer Ordering of Chain Molecules". J. Phys. Chem. B. 2001. 105(39): 9503–9508.
49. G.M. Santos, S. Baldelli. "Monitoring Localized Initial Atmospheric Corrosion of Alkanethiol-Covered Copper Using Sum Frequency Generation Imaging Microscopy: Relation Between Monolayer Properties and Cu_2O Formation". J. Phys. Chem. C. 2013. 117(34): 17591–17602.
50. M. Fang, S. Baldelli. "Surface-Induced Heterogeneity Analysis of an Alkanethiol Monolayer on Microcrystalline Copper Surface Using Sum Frequency Generation Imaging Microscopy". J. Phys. Chem. C. 2017. 121(3): 1591–1601.
51. A. Ulman. "Formation and Structure of Self-Assembled Monolayers". Chem. Rev. 1996. 96(4): 1533–1554.
52. M.W. Tsao, C.L. Hoffmann, J.F. Rabolt, et al. "Studies of Molecular Orientation and Order in Self-assembled Semifluorinated n-Alkanethiols: Single and Dual Component Mixtures". Langmuir. 1997. 13(16): 4317–4322.
53. K.L.A. Cimatu, S. Baldelli. "Spatially Resolved Surface Analysis of an Octadecanethiol Self-Assembled Monolayer on Mild Steel Using Sum Frequency Generation Imaging Microscopy". J. Phys. Chem. C. 2007. 111(19): 7137–7143.
54. Z. Guo, W. Zheng, H. Hamoudi, et al. "On the Chain Length Dependence of CH3 Vibrational Mode Relative Intensities in Sum Frequency Generation Spectra of Self Assembled Alkanethiols". Surf. Sci. 2008. 602(23): 3551–3559.
55. A.D. Curtis, S.R. Burt, A.R. Calchera, et al. "Limitations in the Analysis of Vibrational Sum Frequency Spectra Arising from the Nonresonant Contribution". J. Phys. Chem. C. 2011. 115(23): 11550–11559.
56. E. Tyrode, J.F. Liljeblad. "Water Structure Next to Ordered and Disordered Hydrophobic Silane Monolayers: A Vibrational Sum Frequency Spectroscopy Study". J. Phys. Chem. C. 2013. 117(4): 1780–1790.
57. D. Verreault, W. Hua, H.C. Allen. "From Conventional to Phase-Sensitive Vibrational Sum Frequency Generation Spectroscopy: Probing Water Organization at Aqueous Interfaces". J. Phys. Chem. Lett. 2012. 3(20): 3012–3028.
58. X.D. Zhu, H. Suhr, Y.R. Shen. "Surface Vibrational Spectroscopy by Infrared-Visible Sum Frequency Generation". Phys. Rev. B. 1987. 35(6): 3047–3050.
59. P.A. Franken, A.E. Hill, C.W. Peters, et al. "Generation of Optical Harmonics". Phys. Rev. Lett. 1961. 7(4): 118–119.

60. K.J. Hüttinger, S. Höhmann-Wien, G. Krekel. "A Method for the Determination of the Acid-Base Interactions and the Work of Adhesion at a Solid–Liquid Interface". J. Adhes. Sci. Technol. 1992. 6(3): 317–331.
61. J.R. Dann. "Forces Involved in the Adhesive Process: II. Nondispersion Forces at Solid–Liquid Interfaces". J. Colloid Interface Sci. 1970. 32(2): 321–331.
62. A.R. Hind, S.K. Bhargava, A. McKinnon. "At the Solid/Liquid Interface: FTIR/ATR—The Tool of Choice". Adv. Colloid Interface Sci. 2001. 93(1–3): 91–114.
63. A. Wieckowski, E.R. Savinova, C.G. Vayenas. Catalysis and Electrocatalysis at Nanoparticle Surfaces. New York: Marcel Dekker, 2003.
64. L. Fu, G. Ma, E.C.Y. Yan. "In situ Misfolding of Human Islet Amyloid Polypeptide at Interfaces Probed by Vibrational Sum Frequency Generation". J. Am. Chem. Soc. 2010. 132(15): 5405–5412.
65. J.F. Liljeblad, E. Tyrode, E. Thormann, et al. "Self-Assembly of Long Chain Fatty Acids: Effect of a Methyl Branch". Phys. Chem. Chem. Phys. 2014. 16(33): 17869–17882.
66. N. Akamatsu, K. Domen, C. Hirose. "SFG Study of Two-Dimensional Orientation of Surface Methyl Groups on Cadmium Arachidate Langmuir–Blodgett Films". J. Phys. Chem. 1993. 97(39): 10070–10075.
67. P.E. Colavita, P.G. Miney, L. Taylor, et al. "Effects of Metal Coating on Self-Assembled Monolayers on Gold. 2. Copper on an Oligo(phenylene-ethynylene) Monolayer". Langmuir. 2005. 21(26): 12268–12277.
68. A.P. Boughton, I. Andricioaei, Z. Chen. "Surface Orientation of Magainin 2: Molecular Dynamics Simulation and Sum Frequency Generation Vibrational Spectroscopic Studies". Langmuir. 2010. 26(20): 16031–16036.
69. X. Chen, Z. Chen. "SFG studies on Interactions Between Antimicrobial Peptides and Supported Lipid Bilayers". Biochim. Biophys. Acta. 2006. 1758(9): 1257–1273.